

# Magnetic and structural characterization and ferromagnetic resonance study of thin film HITPERM soft magnetic materials for data storage applications

H. Okumura<sup>a)</sup>

*Department of Electrical and Computer Engineering, Carnegie Mellon University, Pittsburgh, Pennsylvania 15213*

D. J. Twisselmann and R. D. McMichael

*National Institute of Standards and Technology, Gaithersburg, Maryland 20899-8552*

M. Q. Huang

*UES Inc., Dayton, Ohio 45432*

Y. N. Hsu

*IC Mechanics, Inc., Pittsburgh, Pennsylvania 15213*

D. E. Laughlin and M. E. McHenry

*Department of Materials Science and Engineering, Carnegie Mellon University, Pittsburgh, Pennsylvania 15213*

(Presented on 12 November 2002)

HITPERM/SiO<sub>2</sub> single and multilayer thin films have been produced using a target composition of (Fe<sub>70</sub>Co<sub>30</sub>)<sub>88</sub>Zr<sub>7</sub>B<sub>4</sub>Cu<sub>1</sub>. The as-deposited HITPERM film contains small bcc (or B2) nanocrystals of volume fraction less than 10% surrounded by an amorphous matrix. The lattice parameter of the nanocrystal is about 5% larger than an equilibrium FeCo phase. The saturation induction determined from FMR measurements ( $1.53 \pm 0.08$  T) is consistent with VSM and SQUID measurements (1.45–1.5 T) and also with as-spun amorphous ribbons (1.55–1.62 T). The Landé *g*-factors ( $2.15 \pm 0.05$ ) are typical of transition metals, particularly, of Fe. The Landau–Lifshitz–Gilbert damping parameters of the single and multilayered films are small ( $\alpha = 0.0055 \pm 0.0004$ ) with each layer acting almost independently. Neither thickness variation of each layer nor the number of stacking significantly affects the damping process in a range of film thicknesses of 50–150 nm, while the coercivities are strongly dependent on those parameters. This supports a notion that the damping parameter is an intrinsic property. © 2003 American Institute of Physics. [DOI: 10.1063/1.1555871]

## I. INTRODUCTION

Data storage systems require high density media, highly sensitive read heads, and high moment write heads. If perpendicular recording systems are introduced, a high moment soft underlayer will be required for magnetic flux concentration. Further, with the continued increase of data rates in magnetic disk drives, the high frequency performance of soft magnetic thin films has become increasingly important. Magnetic structures modulated with insulating layers that limit eddy currents can have excellent high frequency magnetic response.

HITPERM is a nanocomposite soft magnet<sup>1</sup> with desirable soft magnetic properties, e.g., permeability:  $\approx 2 \times 10^3$  at 2 kHz, saturation induction: 1.5–1.9 T,<sup>2</sup> coercivity: 20–200 A/m, magnetic transition temperature:  $\approx 970$  °C (nanophase),  $\approx 730$  °C (amorphous by extrapolation) and the potential for induced anisotropy achieved by field annealing. FINEMET, NANOPERM and HITPERM nanocrystalline magnetic ma-

terials have been discussed for a variety of applications.<sup>3</sup> Averaging magnetocrystalline anisotropy over grains coupled within an *exchange length* is at the root of magnetic softness in these materials.<sup>4</sup> Of these materials, HITPERM has the largest induction and the highest temperature to which the nanocrystals remain coupled.<sup>5</sup>

In this work, HITPERM/SiO<sub>2</sub> single and multilayer thin films with a various number of layers and thicknesses have been produced. The films were investigated using transmission electron microscopy (TEM) and high resolution TEM (HRTEM), vibration sample magnetometry (VSM) and superconducting quantum interference (SQUID) magnetometry, and ferromagnetic resonance (FMR). The first experimental studies of the high frequency response of HITPERM laminates and the microstructural observations are reported on the sputtered HITPERM films that contain small volume fractions of nanocrystallites. The results indicate a bulk-like damping behavior of the films. The new crystallization observations suggest possibilities for obtaining larger volume fractions of the nanocrystalline phase with small grain sizes, i.e., for desirable soft magnetic films.

<sup>a)</sup>Electronic mail: okumura@ece.cmu.edu

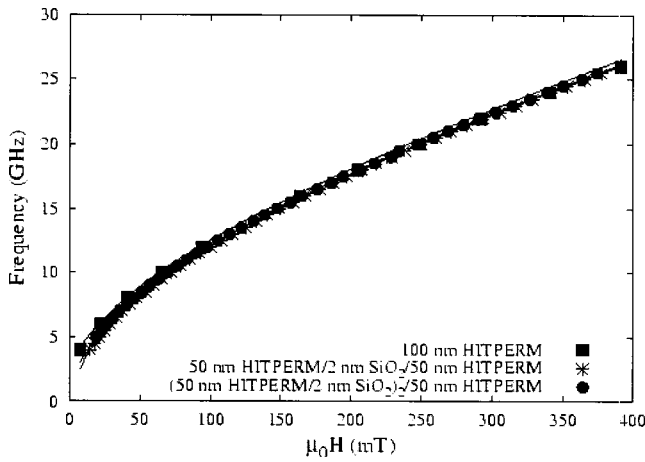


FIG. 1. Ferromagnetic resonance frequency plotted as a function of in-plane FMR resonance fields for various HITPERM thin films.

**II. EXPERIMENT**

The *a*-HITPERM (*a*HTP = amorphous HITPERM) thin films of single layers or *a*HTP/SiO<sub>2</sub>/*a*HTP multilayers, were deposited on glass or Si (100) substrates using a Leybold-Heraeus Z400 rf-sputtering system<sup>6</sup> with a target composition of (Fe<sub>70</sub>Co<sub>30</sub>)<sub>88</sub>Zr<sub>7</sub>B<sub>4</sub>Cu<sub>1</sub>. The letter *N* designates the number of SiO<sub>2</sub> layers. The sputtering conditions used were an Ar pressure of 10 mTorr (1.33 Pa), a sputtering power density of 2.3 W/cm<sup>2</sup> (23 kW/m<sup>2</sup>), and a substrate temperature of ≈24 °C.

The high frequency properties of HITPERM were characterized using ferromagnetic resonance (FMR). By measuring the in-plane FMR resonance field *H*<sub>res</sub>, as a function of resonance frequency  $\omega$ , the effective magnetization *M*<sub>eff</sub>, and Landé *g* factor (spectroscopic splitting factor)  $g = \gamma\hbar/\mu_B$  ( $\gamma$  is the gyromagnetic constant) are determined through a fit to

$$\omega = \gamma\mu_0[(M_{\text{eff}} + H_{\text{res}})(H_{\text{res}} + H_k)]^{1/2}, \tag{1}$$

where  $\mu_0$  is the permeability of vacuum and *H*<sub>*k*</sub> is the anisotropy field. The peak-to-peak linewidth  $\Delta H$  from the same data set gives the Landau–Lifshitz–Gilbert (LLG) damping parameter,  $\alpha$ , via

$$\alpha = \frac{\sqrt{3}}{2} \gamma \frac{d\Delta H}{d\omega}. \tag{2}$$

Magnetic properties at room temperature were measured using a B-H loop tracer with applied fields up to 100 Oe (8 kA/m) at a frequency of 2 Hz. A SQUID magnetometer was also used for the saturation magnetization and the magnetic properties at 5–300 K. JEOL JEM2000-EXII and Philips TECNAI-F20 transmission electron microscopes were employed to study the microstructure of the films.

**III. RESULTS AND DISCUSSION**

Several single and multilayer samples were examined with FMR. Each exhibited similar in-plane frequency dependence of *H*<sub>res</sub> (Fig. 1) although the one multilayer sample [50 nm(*a*TP)/2 nm(SiO<sub>2</sub>)/50 nm(*a*HTP)] exhibited two peaks at high frequencies; the individual layers being resolved independently. By fitting these curves to Eq. (1), we obtain val-

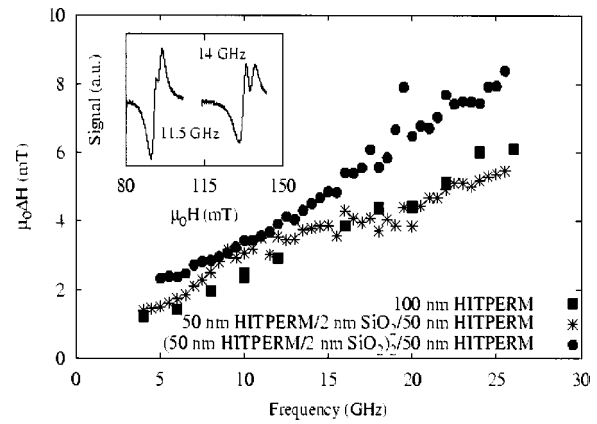


FIG. 2. Peak-to-peak linewidth plotted as a function of in-plane FMR frequency for various HITPERM films.

ues for *M*<sub>eff</sub> and *g* as given in Table I. There is good agreement between samples, with average values of  $g = 2.15 \pm 0.05$  and  $\mu_0 M_{\text{eff}} = 1.53 \pm 0.08$  T. The Landé *g* factors are typical of transition metals [Fe(2.12–2.17), Co(2.22), Ni(2.20)], particularly, of Fe, and the saturation induction values are consistent with VSM and SQUID measurements (1.45–1.5 T) of the films and also as-spun amorphous ribbons (1.55–1.62 T). The slightly smaller values for the films are probably due to bonding at the interface (magnetic dead layer).

Figure 2 shows in-plane frequency dependence of  $\Delta H$  for three samples, 100 nm HITPERM, [50 nm(*a*HTP)/2 nm(SiO<sub>2</sub>)]<sub>2</sub>/50 nm(*a*HTP) and 50 nm(*a*HTP)/2 nm(SiO<sub>2</sub>)/50 nm(*a*HTP). The linewidths of the single layer film and the trilayer depend linearly on frequency. The bump, from approximately 7.5 to 15 GHz in the 50 nm bilayer data, is due to the two overlapping peaks, which combine to give an effectively larger linewidth, but which is not indicative of increased damping. Sample spectra are shown in the inset of Fig. 2. Above approximately 15 GHz, the two peaks are sufficiently separated to resolve, upon which the linewidth and slope return to values similar to those for a single layer film. The increased slope for the trilayer stack (as compared to single and bilayer films) is interpreted similarly, i.e., three overlapping peaks which are never separated enough to be resolved from each other, but which do combine to give an increased linewidth and thus a higher calculated value of  $\alpha$ . Accounting for these effects, an  $\alpha$  value of  $0.0055 \pm 0.0004$  was determined.

The damping parameters obtained above are significantly smaller than often reported values for thin films.<sup>7,8</sup> Also, neither thickness variation of each layer nor the num-

TABLE I. Landé *g*-factor (spectroscopic splitting factor) *g*, effective magnetization *M*<sub>eff</sub>, and the Landau–Lifshitz–Gilbert damping parameter  $\alpha$ , of various HITPERM films obtained from FMR studies.

<i>t</i> (nm)	<i>g</i>	$\mu_0 M_{\text{eff}}$ (T)	$\alpha$
100	2.06	1.66	0.0058
150	2.16	1.51	0.0055
50/2/50	2.14	1.56	0.0050
100/4/100	2.21	1.47	0.0058
50/2/50/2/50	2.19	1.47	0.0082

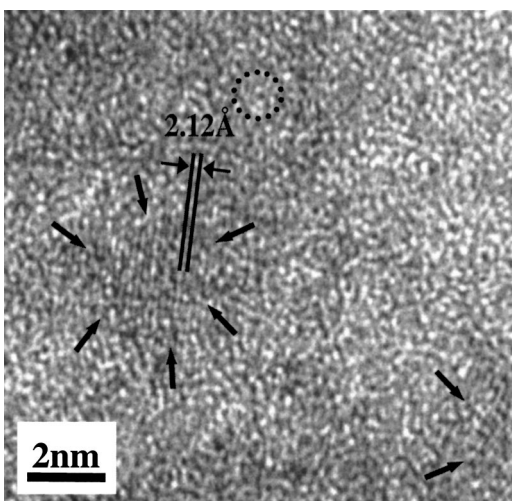


FIG. 3. HRTEM image of an as-sputtered HITPERM thin film. Arrows indicated the boundary between the amorphous matrix and the nanoparticle.

ber of stacking significantly affects the damping process in a range of film thicknesses of 50–150 nm. This is consistent with the observed small damping parameters, which are often found for bulk materials,<sup>9</sup> supporting a notion that the damping parameter is an intrinsic property. However, the coercivity of the film is strongly structure-sensitive.<sup>10</sup> The fast flux reversal in the multilayers may be due to the magnetostatic coupling field originating from the ripple structure (the effective anisotropy field decreases)<sup>11,12</sup> but the details are not known. It is also worth noting that the small difference of the damping parameter among layers may be due to the slightly different anisotropy in each layer, which is supported by low temperature SQUID measurements where the hysteresis loop exhibits a clear step in the demagnetization curve (but the step disappears with temperature).<sup>10</sup>

HRTEM studies on the as-deposited HITPERM films reveal extremely small bcc (or B2) nanocrystals with the diameter of a few nanometers surrounded by amorphous matrix (see Fig. 3), where the arrows indicate the boundary between the nanocrystals and the amorphous matrix. From the lattice fringes of the nanocrystals, the plane distance is estimated to be around 0.212 nm, about 5% larger than the expected  $d$ -spacing of the FeCo (110) plane [ $a(\text{FeCo}) = 0.28486$  nm for a bcc disordered phase and  $a(\text{FeCo}) = 0.28504$  nm for a B2 ordered structure]. The volume fraction of the nanocrystals is, by assuming spherical particles, roughly estimated to be  $\approx 8\%$  according to both two-dimensional and three-dimensional approximations. Although the amorphous contrast is mostly observed outside the nanocrystals, a medium range order (MRO)-like structure is sometimes seen even in the amorphous region, an example of which is also indicated in Fig. 3 by a dotted circle.

The premier magnetic properties in HITPERM are derived from the two-phase microstructure consisting of nanocrystalline ferromagnetic grains surrounded by a ferromagnetic amorphous matrix. Although the above as-deposited HITPERM films have a low volume fraction of nanocrystals, preliminary results on *in situ* heat treated and postannealed thin films show the magnetic properties are good or even

better when the amount of nanocrystals is increased. One important advantage of the HITPERM alloy is that the nanocrystals and the amorphous matrix are both magnetic even at elevated temperatures. They are ferromagnetically exchange coupled above the nanocrystallization temperature (the estimated Curie temperature of amorphous  $\approx 730$  °C). By producing the grain size of the nanocrystalline phases much smaller than the magnetic exchange length (on an order of 100 nm), the magnetocrystalline anisotropy and magnetostriction would be averaged out over the many small grains<sup>3</sup> even at elevated temperatures, which would lead to desirable soft magnetic materials for high temperature applications.

Dark field TEM images clearly show homogeneous distribution of those ultrafine crystals, as well as some clusters that tend to agglomerate with each other. The chemical partitioning process, which is required for crystallization of FeCo(-rich) phase grains and the grain growth, should be significantly facilitated with the existence of such clusters. Since *in situ* TEM experiments using a hot stage sample holder shows crystallization below 400 °C (some start even around 370 °C), which is significantly lower than a bulk nanocrystallization temperature of  $\approx 500$  °C, these clusterings in thin films might play an important role when the specimen temperature is raised and the atomic diffusion becomes active. The significantly low crystallization temperature might be due to the high surface energy and large strains in thin films assisting the diffusion of atoms through the larger atomic mobility (due to the ease of accommodation of the strains in TEM/thin film samples).

Electron diffraction images are also consistent with the above observations, showing an amorphous halo pattern that coincides with the weak bcc (or B2) (110) rings from the nanocrystals. The estimated lattice parameter of cubic phase is about 0.300 nm or 5% larger than B2 FeCo, which is consistent with the HRTEM observations. The FeCo lattice spacing increase in the incipient FeCo nanocrystals may be due to entrapped Zr atoms (substitutionally) and/or B atoms (interstitially) in the nanoparticles, but the detailed analysis is required for further elucidation of the chemical partitioning process.

<sup>1</sup>M. A. Willard, D. E. Laughlin, and M. E. McHenry, J. Appl. Phys. **87**, 7091 (2000).

<sup>2</sup>H. Iwanabe, B. Lu, M. E. McHenry, and D. E. Laughlin, J. Appl. Phys. **85**, 4424 (1999).

<sup>3</sup>M. E. McHenry, M. A. Willard, and D. E. Laughlin, Prog. Mater. Sci. **44**, 291 (2001).

<sup>4</sup>G. Herzer, IEEE Trans. Magn. **26**, 1397 (1990).

<sup>5</sup>F. Johnson, P. Hughes, R. Gallagher, D. E. Laughlin, M. E. McHenry, M. A. Willard, and V. G. Harris, IEEE Trans. Magn. **37**, 2261 (2001).

<sup>6</sup>The identification of any commercial product or trade name does not imply endorsement or recommendation by the National Institute of Standards and Technology.

<sup>7</sup>E. B. Myers, D. C. Ralph, J. A. Katine, R. N. Louie, and R. A. Buhrman, Science **285**, 867 (1999).

<sup>8</sup>C.H. Back, R. Allenspach, W. Weber, S. S. P. Parkin, D. Weller, E. L. Garwin, and H. C. Siegmund, Science **285**, 864 (1999).

<sup>9</sup>Y. Tserkovnyak and A. Brataas, Phys. Rev. Lett. **88**, 117601 (2002).

<sup>10</sup>M. Q. Huang, Y. N. Hsu, M. E. McHenry, and D. E. Laughlin, IEEE Trans. Magn. **37**, 2239 (2001).

<sup>11</sup>R. Hasegawa, Phys. Status Solidi A **5**, 375 (1971).

<sup>12</sup>R. Hasegawa, Phys. Status Solidi A **5**, 661 (1971).